NANO LETTERS

pubs.acs.org/NanoLett Letter

Rewritable Photonic Integrated Circuit Canvas Based on Low-Loss Phase Change Material and Nanosecond Pulsed Lasers

Forrest Miller, Rui Chen, Johannes Fröch, Zhuoran Fang, Virat Tara, Sarah Geiger, and Arka Majumdar*

Cite This: *Nano Lett.* 2024, 24, 6844−6849 Read Online

ACCESS | Metrics & More | Article Recommendations | Supporting Information

ABSTRACT: Programmable photonic integrated circuits (PICs) are an increasingly important platform in optical science and engineering. However, current programmable PICs are mostly formed through subtractive fabrication techniques, which limits the reconfigurability of the device and makes prototyping costly and time-consuming. A rewritable PIC architecture can circumvent these drawbacks, where PICs are repeatedly written and erased on a single PIC canvas. We demonstrate such a rewritable PIC platform by selective laser writing a layer of wide-band-gap phase change material (PCM) Sb_2S_3 with a low-cost benchtop setup. We show arbitrary patterning with resolution up to 300 nm and write dielectric assisted waveguides with a low optical loss of 0.0172 dB/μm. We envision that using this inexpensive benchtop platform thousands of PIC designs can be written, tested, and erased on the same chip without the need for lithography/etching tools or a nanofabrication facility, thus reducing manufacturing cost and increasing accessibility.

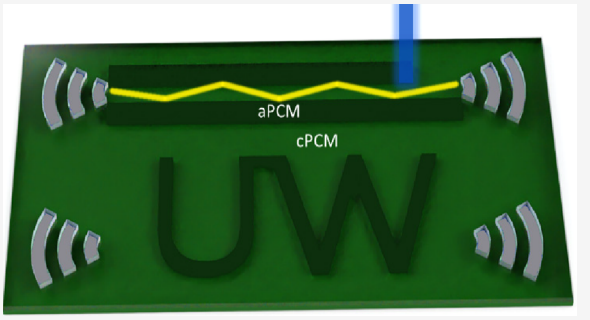

KEYWORDS: *rewritable photonic integrated circuits, phase-change materials, low loss, laser writing*

Photonic integrated circuits (PICs) have found a plethora of applications in optical communication, sensing, and information processing.[1−3] Programmability is a key feature in these PICs,[4,5] which enables multiple functionalities on the same PIC chip. To change their functionality, conventional programmable PICs[6,7] rely on fabricated on-chip active components, such as phase shifters and tunable absorbers. However, the PIC architectures are fixed once fabricated due to the subtractive fabrication process. This limits the scope of the PIC's programmability. Alternatively, rewritable PICs[8] that can be written and erased reversibly have no limitation to their realized programmability except for the writing capability of the tool.

Nonvolatile chalcogenide phase change materials (PCMs)[6,9,10] offer a promising platform to realize rewritable PICs. PCMs are a class of materials whose refractive index changes dramatically ($\Delta n \sim O(1)$) based on the microstructural arrangement of their constituent atoms.[10] This arrangement is either an ordered crystalline lattice (c-phase) or an amorphous Brownian arrangement (a-phase). Since both states are stable under the ambient environment, no external energy is required after the phase transition is triggered. When held above the glass transition temperature for sufficient time, the atoms in a PCM form the thermodynamically favored c-phase (crystallization). Conversely, the metastable a-state can be reached through a melt-quench process (amorphization), in which the atoms do not have sufficient time to form a crystalline lattice before their lack of energy renders them immobile. This lack of mobility forms an energy barrier that makes both the a-state and c-state nonvolatile. One practical way to amorphize the PCMs is through short optical pulses,[11] while crystallization can be achieved by annealing PCMs on a hot plate[12] or longer optical pulses.[13]

Laser-written PCM metasurfaces or metalenses have been demonstrated using femtosecond[14−17] or nanosecond laser pulses,[18] but optical loss is not critical in these applications since the light only interacts with PCMs over a short distance (<100 nm). In contrast, loss becomes paramount for PICs due to the much longer millimeter or even centimeter propagation length.[19] Well-known PCMs, such as GST or GSST, provide high index contrast ($\Delta n \sim 3$) at the near-infrared (NIR) wavelength range, but they are also prohibitively lossy ($\kappa \sim 0.5$).[6,20] Fortunately, recently reported low-loss PCMs with wider bandgaps, such as antimony sulfide (Sb_2S_3) and antimony selenide (Sb_2Se_3)[21] have emerged as promising alternatives. Their wider bandgaps lead to much weaker material absorption in the NIR ($\kappa \sim 0$ at 1550 nm) with a relatively large index contrast ($\Delta n \sim 0.6$).[21] Enormous endeavors have been made to integrate these low-loss PCMs onto mature PIC platforms such as Si[7,22−24] or Si_3N_4[25] on

Received: January 5, 2024
Revised: May 20, 2024
Accepted: May 22, 2024
Published: May 28, 2024

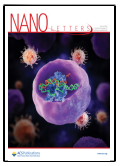

https://doi.org/10.1021/acs.nanolett.4c00070
Nano Lett. 2024, 24, 6844−6849

insulator. However, these devices are still conventional programmable PICs with programmability limited by the immutable PIC architecture.

Here, we experimentally demonstrate a low-loss and rewritable PIC platform using laser-written Sb_2S_3. A dielectric-assisted waveguide structure[8,26] is used to lower the optical propagation loss while enhancing the endurance and reliability of PCMs. We first demonstrate arbitrary patterning on the PCM canvas with a fine resolution of 600 nm line pitch, to demonstrate the rewritable capability of our platform, then write laser-written waveguides between pairs of predefined grating couplers. This is achieved by amorphizing the c-Sb_2S_3 using an inexpensive nanosecond pulsed laser to form low index a-Sb_2S_3 cladding around the high index c-Sb_2S_3 core. The propagation loss was then measured via a cutback measurement as 0.01722 dB/μm, comparable to the 0.010 dB/μm loss in simulation.[8] While this loss is ∼1000 times larger than current commercial silicon photonic waveguides,[27] this loss is acceptable to create waveguides of submm length. Our rewritable and low-cost platform shows a promising path to democratizing PIC prototyping for designers without access to a nanofabrication facility, which will enhance PIC education and accelerate rapid PIC prototyping.

Figure 1a shows the schematic of our rewritable PIC setup, where an Sb_2S_3-based rewritable PIC canvas was written with a nanosecond pulsed laser (write laser) and a three-axis motor stage (see Supplementary Section S1 for our experimental setup). The PIC canvas was fabricated by depositing multiple materials on a silicon substrate in the order of 3.5 μm SiO_2, 15 nm Sb_2S_3, 20 nm Al_2O_3 and 400 nm Si_3N_4 (see Supplementary Section S2 for fabrication process steps), as shown in the inset of Figure 1a. This multilayer design enables the low-loss dielectric-assisted waveguide mode (see Supplementary Figure S2)[8] and is key to low-loss waveguiding. We started with a c-Sb_2S_3 PIC canvas by annealing the chip at 325 °C on a hot plate. Patterns or waveguides were formed by amorphizing the Sb_2S_3 using the nanosecond pulsed laser and were erased by another hot plate annealing. To measure the written PIC devices, probe light with a wavelength of 1465 nm was coupled in and out of the chip through prefabricated Si_3N_4 grating couplers (see Supplementary Section S3) for high-efficiency probing of the waveguiding phenomena. The waveguides or arbitrary photonic structures can be written and erased between the grating coupler pairs. These predefined grating couplers could be removed since the gratings can be made out of the PCM itself,[13] but the coupling efficiency in our case remains inferior to an etched grating. The optical response of the laser-written devices was then measured via a vertical fiber coupling setup.

We first tested various laser pulse conditions and identified suitable ones (see Supplementary Section S4). The laser-switched areas were verified as a-Sb_2S_3 using Raman spectroscopy. Multiple laser conditions could amorphize Sb_2S_3, and we chose pulses with a duration of 13 ns and peak power of 50 mW for this experiment. Of the viable pulses and peak powers, we chose the second shortest pulse setting, 13 ns, and the second lowest peak power, 50 mW, to have reliable switching while maintaining a short exposure time. The short exposure ensures the amorphous state is favored after irradiation, while the low power reduces the chances of material degradation such as Rayleigh instability.

The diffraction-limited resolution of our setup is estimated to be 250 nm with our 450 nm laser and a 0.9 numerical aperture (NA) objective lens. We note that the minimum step size of the stage is 100 nm, so the resolution could be further improved with a shorter laser wavelength or a higher NA objective. We then characterized the resolution experimentally by laser writing a resolution chart consisting of sets of vertical lines with varying pitch. Figure 2 (left) shows the optical micrograph of the chip after laser writing and the pixel values along the solid black line are plotted in Figure 2 (right). The prominence of the peaks starts to decrease at ∼700 nm line pitch and is not reliably distinguishable for a 500 nm pitch. The lines with 600 nm pitch are differentiable from the background but are marginal in the optical contrast. Therefore, we consider a 600 nm line pitch as the maximum resolution of our setup. This corresponds to a 300 nm spot size, close to the diffraction limit of 250 nm. With this relatively high resolution, it is possible to pattern devices, such as ring resonators, Mach–Zehnder interferometers, and grating couplers. It is worth noting that Figure 2 was taken on an optical microscope, whose diffraction limit also potentially limits the resolution characterization.

A helpful property of Sb_2S_3 for laser writing is its slow crystallization speed.[7] This implies that the amorphous state is heavily favored during the sharp thermal transients of laser heating. Therefore, the same region of Sb_2S_3 can be exposed multiple times without switching amorphous Sb_2S_3 back into

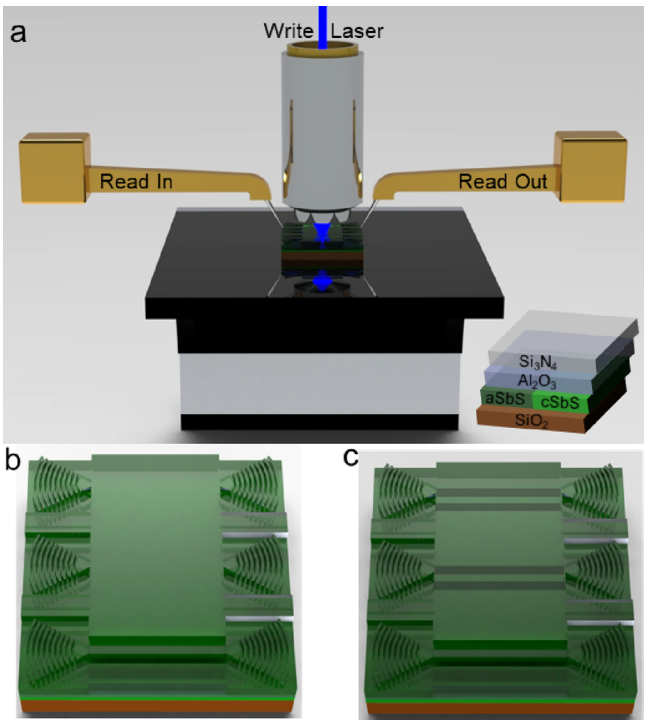

Figure 1. Rewritable photonic integrated circuit platform based on the low-loss PCM Sb_2S_3 with dielectric-assisted waveguide structure patterned by cost-efficient nanosecond pulsed lasers and translation stage. (a) A schematic rendering of the rewritable chip on a stage. The write laser switches Sb_2S_3 from the crystalline to amorphous state to form PICs, and then the read probes measure the PIC. (b) An erased rewritable chip with no features between the grating coupler pairs. (c) A rewritable chip with two laser-written waveguides connecting the top two pairs of waveguides. The bottom pair of waveguides is connected with an etched Si_3N_4 waveguide and is used as a reference for power normalization. In the experiment, our chip had more than 200 pairs of grating couplers (see Supplementary Figure S8), allowing many more structures to be written than depicted here.

https://doi.org/10.1021/acs.nanolett.4c00070
Nano Lett. 2024, 24, 6844−6849

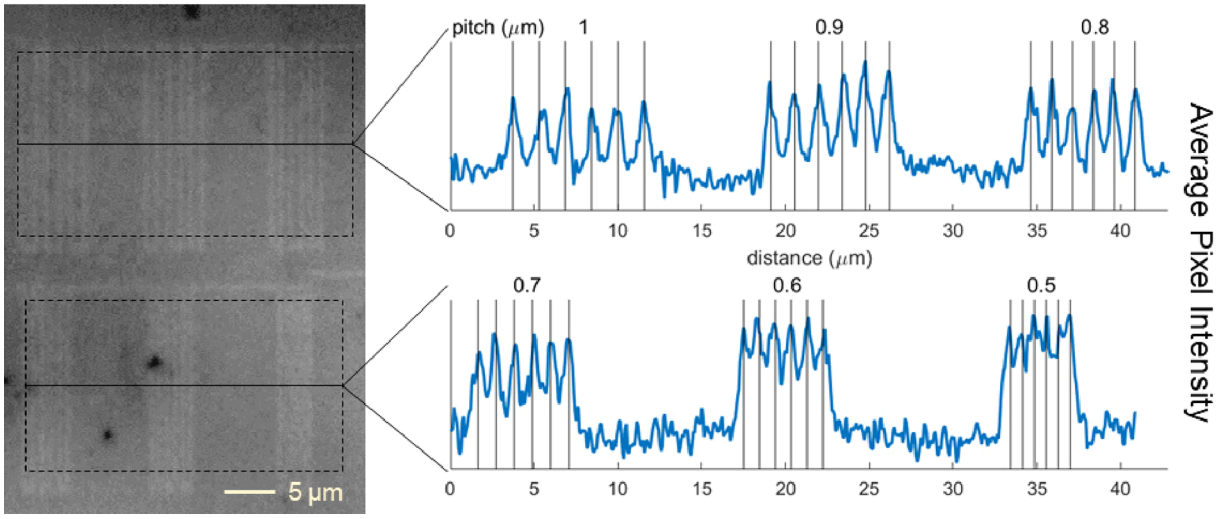

Figure 2. Resolution test with laser-written line pairs. (Left) A micrograph image of vertical lines with a fixed duty cycle of 50% and varying pitches, ranging from 1000 to 500 nm. The white lines are laser-amorphized regions. (Right) Intensity along the solid lines on the left figure. The results are averaged along the *y* direction in the dashed boxes. The pitch of the lines is listed above each plot.

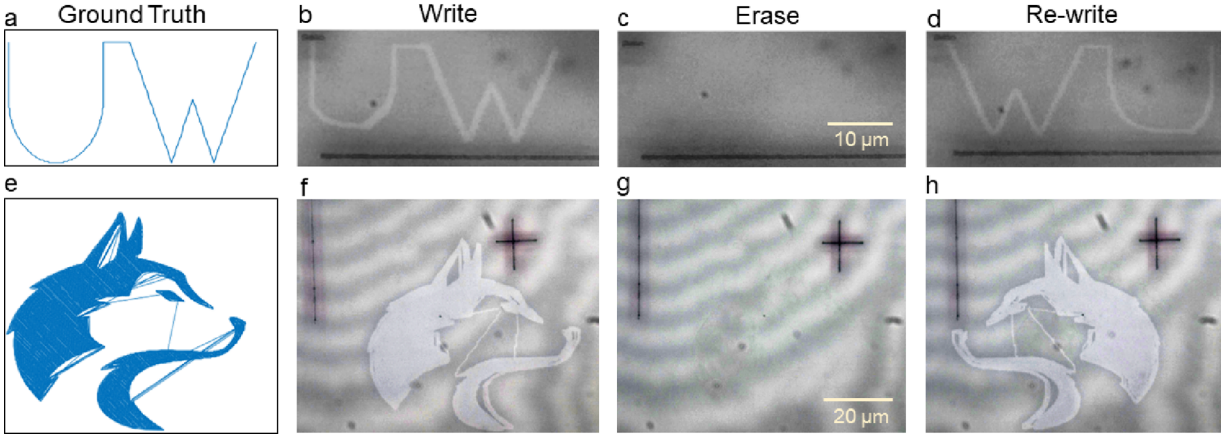

Figure 3. Reversible writing of different patterns at the same region of the Sb_2S_3 canvas. (a) The ground truth of the letters "UW", (b) the optical microscope image after the "UW" pattern was written and (c) erased, and (d) the letters "WU" were written at the same region. (e–h) An image of a husky written, erased, then rewritten but reflected across the *y*-axis.

the crystalline state. We used this multipass scheme to achieve a more uniform pattern for the waveguide structures exceeding 0.7 mm. For these longer waveguides, the areas around the grating couplers could undergo inconsistent switching due to focus drift over the long travel distance. These areas were re-exposed no more than a total of 3 times to ensure the structure guided the light as it exited the grating coupler.

Figure 3 shows two patterns which were written over a period of 2 and 25 min, respectively. In the top (bottom) row, we show a pattern of the letters "UW" (a husky picture), consisting of 88 (over 9,000) coordinate pairs. The patterns were written on a pristine area of c-Sb_2S_3, then the sample was annealed on a hot plate to recrystallize the Sb_2S_3 under 325 °C. A reflection of the same pattern was then written over the same region of Sb_2S_3. The black lines and crossings in the figures are laser-ablated regions to show that the writing region is unchanged. Although we only demonstrate two cycles of rewritability, Sb_2S_3 can be reversibly switched at least 2000 times.[21] This high endurance, paired with the capability of arbitrary patterning, would enable thousands of PICs to be written and tested on the same chip, enabling rapid prototyping of PIC devices and systems.

Writing the low-loss waveguide requires aligning the laser spot to the edge of the grating coupler. A rotational stage was used to iteratively correct any rotational misalignment by aligning the laser spot to the edges of the left and the right grating couplers multiple times. After the alignment and rotational correction, the 3-axis stage executed a preprogrammed serpentine pattern to write each waveguide cladding. During the laser writing, a dynamic focusing script adjusted the objective height to keep the focal spot in the same plane as the chip. A 500-μm-long waveguide took approximately 30 min to write. We anticipate that the process could be accelerated by more than a factor of 4 using an objective with a lower NA of 0.2 to achieve a larger spot size. Additionally, the larger depth of field in a lower NA objective would reduce the chance of ragged waveguide claddings from mechanical instability, allowing the stage to translate faster without reducing the reliability of the system.

In total, 18 waveguides were written, with three waveguides of length 500, 600, 700, 800, 900, and 1000 μm. Each

https://doi.org/10.1021/acs.nanolett.4c00070
Nano Lett. 2024, 24, 6844–6849

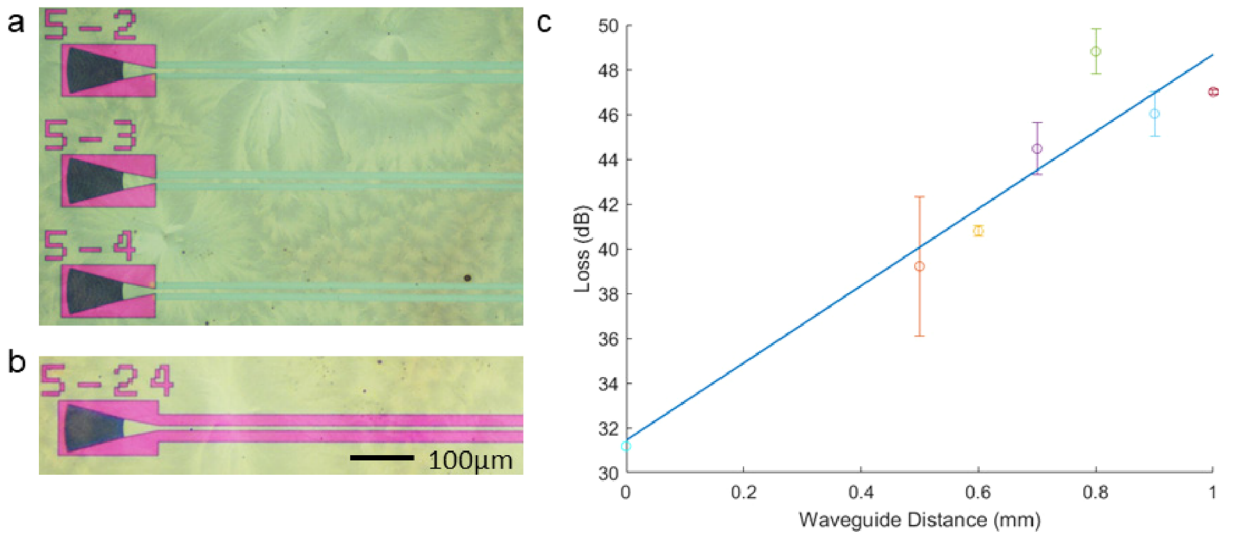

Figure 4. Laser-written waveguides on the rewritable Sb_2S_3 PIC canvas. (a) Optical micrograph for the laser-written waveguides connecting two predefined grating couplers. Only the left grating coupler is shown in the picture. (b) Optical micrograph of the etched Si_3N_4 waveguide which was used as the reference. (c) Plot of the mean loss for different waveguide lengths. The 0.0172 dB/μm slope matches the theoretical value of 10 dB/mm well. The y-intercept was set by the 500 μm etched waveguide, assuming the Si_3N_4 waveguides were lossless.

waveguide was given a cladding at least 3 μm wide and a core width of 3−4 μm. The core width was designed to be 2.5 μm, but alignment to the 4-μm-wide grating coupler taper was more reliable than centering the written pattern by hand. Additionally, this mismatch between the laser-written core width and the grating coupler end width could cause reflection at the interface, contributing additional and variable optical loss. After laser writing, the waveguides were measured through a cut-back measurement in which waveguides of different lengths were written and their losses compared. Each waveguide was normalized to a Si_3N_4 reference waveguide, fabricated through etching on the same column. Figures 4a and 4b shows optical micrograph images of the laser-written waveguides and the Si_3N_4 reference waveguide (more images can be found in Supplementary Section S5).

To verify the waveguiding effect, we compare the laser-written waveguides with blank grating pairs with no waveguides written between them. The written waveguides increased transmission by an average of 9.93 dB compared with the blank gratings (see Supplementary Section S6), showcasing waveguiding behavior within the c-Sb_2S_3 core. We note that the grating demonstrated the most consistent coupling efficiency at 1465 nm (see Supplementary Figure S5), which was the wavelength used in the cutback measurement.

We then characterized the unit loss of the laser-written integrated waveguide. Figure 4c shows the cutback measurement results, where the measured power transmission of the written waveguides was averaged among three samples for each waveguide length. The measured transmission spectra from 1420 to 1500 nm can be found in Supplementary Figure S5. Assuming the reference Si_3N_4 waveguides are lossless, we estimate the coupling efficiency as 15.5 dB/facet, indicated by the y-intercept. The error bar represents the standard deviation, with the average standard deviation being 1.1 dB. A linearly fitted trendline had a slope of 17.2 dB/mm, which matched well with the theoretical value of 10 dB/mm.[8] This variation could be attributed to several factors, such as (1) the anisotropy of c-Sb_2S_3 crystals, (2) mode leakage during propagation, (3) variation in the grating couplers, (4) misalignment between the axis of the writing laser and the chip, and (5) variation in the waveguide widths and cladding thicknesses. Among the etched Si_3N_4 waveguides, there was a standard deviation from the mean of 3.5 dB, implying variation in the material and gratings. The remaining error is likely from mode leakage or experimental nonidealities. The mode confinement could be improved with a thicker Sb_2S_3 layer, and we show that 45 nm Sb_2S_3 could also be laser amorphized (see Supplementary Figure S10). We note that although traditional SOI waveguides typically suffer from loss due to surface roughness, our PCM canvas is less susceptible. Such loss is due to Rayleigh scattering, which decreases with lower refractive index contrast between the core and cladding. In our case, the refractive index contrast is ∼0.6 in only a thin layer of Sb_2S_3, so the scattering is significantly smaller than conventional SOI waveguides. Moreover, the laser writing system creates a gradual index change at the boundary, further reducing the confinement factor and hence the scattering loss. As for the roughness itself, the rectilinear movement of our stage was smooth and any ragged edges due to focus drift were corrected with multiple passes.

In this work, we demonstrated low-loss, laser-written waveguides in a nonvolatile PCM platform using inexpensive benchtop components (setup cost < $22,000) that in total are 50X less expensive than the mask writing laser used in other works.[13,28] We also demonstrate the first rewritable PIC platform using the wide band gap PCM Sb_2S_3, which can enable PICs operating in the near-visible spectrum range (∼800 nm). Our platform exhibits a high patterning resolution of 300 nm with reversible and arbitrary patterning capability. Additionally, we demonstrated rewritable waveguides using a dielectric-assisted waveguide structure, showcasing a low propagation loss of 0.0172 dB/μm, close to the theoretical value of 0.01 dB/μm.

Our current PCM canvas is optimized for low-loss operation and does not support waveguide bends. This follows from the fundamental trade-off between the propagation loss and the mode confinement, incurred by the finite extinction coefficient

https://doi.org/10.1021/acs.nanolett.4c00070
Nano Lett. 2024, 24, 6844−6849

of Sb_2S_3.[8] A thicker Sb_2S_3 film leads to a more confined optical mode, but at expense of a higher propagation loss due to the increased mode interaction with lossy c-Sb_2S_3 (see optical mode simulation in Supplementary Section S1). To mitigate this loss-confinement trade-off and enable sufficient confinement for waveguide bends, we need to further reduce the loss of the PCM canvas. One approach is to reduce the scattering loss due to the domain boundary scattering of polycrystalline Sb_2S_3, which can be mitigated by engineering the pulsed laser conditions to reduce the loss. For example, one can guide the crystal growth direction by laser writing crystallization instead of hot plate to reduce the boundary.[13] Alternatively, since our PCM laser writing platform is PCM transferrable, another approach is to use other low-loss PCMs such as Sb_2Se_3, which provides a much better mode confinement with lower loss (See Supplement Section S8 for further comparison between Sb_2S_3 and Sb_2Se_3). These properties significantly improve the bend radius/propagation loss trade-off. Future works should strive to demonstrate other functional devices, such as directional couplers, multimode interferometers, ring resonators, and grating couplers, either in Sb_2S_3 or Sb_2Se_3, to demonstrate further functionality on our platform.

Looking forward, the experimentally demonstrated rewritable PIC canvas represents a new direction for PIC development. Fabricating and testing photonic structures no longer requires weeks of work by highly trained students/technicians, specialized environments, or million-dollar equipment. Our work enables etch-less and recyclable PIC fabrication, which is crucial to accelerating the PIC prototyping cycle, reducing cost, and expanding the field of PIC research to researchers without nanofabrication facilities. We anticipate that expanding the pool of PIC researchers will lead to more innovative ideas, and the experimentally tested layouts will result in higher confidence for designs that are sent to fabs for their final realization.

■ ASSOCIATED CONTENT

Supporting Information

The Supporting Information is available free of charge at https://pubs.acs.org/doi/10.1021/acs.nanolett.4c00070.

Experimental setup details, simulated mode profiles of Sb_2S_3 waveguides, fabrication process for Sb_2S_3-based rewritable canvas, grating coupler design, Raman spectra to verify PCM phase change, additional optical microscope images of switched devices, loss discussion, measurement results to compare our waveguiding to unguided transmission, and discussion on thicker PCM switching and curved structures (PDF)

■ AUTHOR INFORMATION

Corresponding Author

Arka Majumdar − *Department of Electrical and Computer Engineering, University of Washington, Seattle, Washington 98195, United States; Department of Physics, University of Washington, Seattle, Washington 98195, United States;* orcid.org/0000-0003-0917-590X; Email: arka@ece.uw.edu

Authors

Forrest Miller − *Department of Electrical and Computer Engineering, University of Washington, Seattle, Washington 98195, United States; Draper Scholar, The Charles Stark Draper Laboratory, Cambridge, Massachusetts 02139, United States;* orcid.org/0009-0000-1840-4204

Rui Chen − *Department of Electrical and Computer Engineering, University of Washington, Seattle, Washington 98195, United States;* orcid.org/0000-0001-8492-729X

Johannes Fröch − *Department of Electrical and Computer Engineering, University of Washington, Seattle, Washington 98195, United States; Department of Physics, University of Washington, Seattle, Washington 98195, United States*

Zhuoran Fang − *Department of Electrical and Computer Engineering, University of Washington, Seattle, Washington 98195, United States;* orcid.org/0000-0001-8724-6633

Virat Tara − *Department of Electrical and Computer Engineering, University of Washington, Seattle, Washington 98195, United States*

Sarah Geiger − *The Charles Stark Draper Laboratory, Cambridge, Massachusetts 02139, United States*

Complete contact information is available at: https://pubs.acs.org/10.1021/acs.nanolett.4c00070

Notes

The authors declare no competing financial interest.

■ ACKNOWLEDGMENTS

F.M. and A.M. conceived the project. F.M. designed the dielectric-assisted waveguide structure and built the rewritable PIC setup with the help of J.F. R.C. fabricated the Sb_2S_3-based rewritable PIC canvas. R.C., Z.F., H.R., V.T., and S.G. helped with the experiment and data processing. A.M. supervised the overall progress of the project. F.M. wrote the manuscript with input from all the authors. F.M. is supported by a Draper Scholarship. This project was funded by the Defense Advanced Research Projects Agency (W911NF-21-10368). Part of this work was conducted at the Molecular Analysis Facility, a National Nanotechnology Coordinated Infrastructure (NNCI) site at the University of Washington, which is supported in part by funds from the National Science Foundation (awards NNCI-2025489, NNCI-1542101), the Molecular Engineering & Sciences Institute, and the Clean Energy Institute.

■ REFERENCES

(1) Wang, K.; et al. High-speed indoor optical wireless communication system employing a silicon integrated photonic circuit. *Opt. Lett.* **2018**, *43* (13), 3132−3135.

(2) He, L.; Li, H.; Li, M. "Optomechanical measurement of photon spin angular momentum and optical torque in integrated photonic devices. *Science Advances* **2016**, *2* (9), No. e1600485.

(3) Wang, J.; Sciarrino, F.; Laing, A.; Thompson, M. G. "Integrated photonic quantum technologies. *Nat. Photonics* **2020**, *14* (5), 273−284.

(4) Bogaerts, W.; et al. Programmable photonic circuits. *Nature* **2020**, *586* (7828), 207−216.

(5) Harris, N. C.; et al. Linear programmable nanophotonic processors. *Optica* **2018**, *5* (12), 1623−1631.

(6) Chen, R.; Fang, Z.; Miller, F.; Rarick, H.; Fröch, J. E.; Majumdar, A. "Opportunities and Challenges for Large-Scale Phase-Change Material Integrated Electro-Photonics. *ACS Photonics* **2022**, *9* (10), 3181−3195.

(7) Chen, R.; et al. Non-volatile electrically programmable integrated photonics with a 5-bit operation. *Nat. Commun.* **2023**, *14* (1), 3465.

(8) Miller, F.; Chen, R.; Froech, J. E.; Rarick, H.; Geiger, S.; Majumdar, A. "Rewritable photonic integrated circuits using

dielectric-assisted phase-change material waveguides. *Opt. Lett.* **2023**, *48* (9), 2385−2388.
(9) Youngblood, N.; Ríos Ocampo, C. A.; Pernice, W. H. P.; Bhaskaran, H. ″Integrated optical memristors. *Nat. Photonics* **2023**, *17* (7), 561−572.
(10) Fang, Z.; Chen, R.; Zheng, J.; Majumdar, A. Non-Volatile Reconfigurable Silicon Photonics Based on Phase-Change Materials. *IEEE J. Sel. Top. Quantum Electron.* **2022**, *28* (3), 1−17.
(11) Ríos, C.; et al. Integrated all-photonic non-volatile multi-level memory. *Nat. Photonics* **2015**, *9* (11), 725−732.
(12) Xu, P.; Zheng, J.; Doylend, J. K.; Majumdar, A. ″Low-Loss and Broadband Nonvolatile Phase-Change Directional Coupler Switches. *ACS Photonics* **2019**, *6* (2), 553−557.
(13) Wu, C.; et al. Freeform direct-write and rewritable photonic integrated circuits in phase-change thin films. *Science Advances* **2024**, *10* (1), No. eadk1361.
(14) Wang, Q.; et al. Optically reconfigurable metasurfaces and photonic devices based on phase change materials. *Nat. Photonics* **2016**, *10* (1), 60−65.
(15) Michel, A.-K. U.; Zalden, P.; Chigrin, D. N.; Wuttig, M.; Lindenberg, A. M.; Taubner, T. ″Reversible Optical Switching of Infrared Antenna Resonances with Ultrathin Phase-Change Layers Using Femtosecond Laser Pulses. *ACS Photonics* **2014**, *1* (9), 833−839.
(16) Smayev, M. P.; et al. Direct single-pass writing of two-phase binary diffraction gratings in a Ge2Sb2Te5 thin film by femtosecond laser pulses. *Optics & Laser Technology* **2022**, *153*, No. 108212.
(17) Dong, K.; et al. ″A Lithography-Free and Field-Programmable Photonic Metacanvas. *Adv. Mater.* **2018**, *30* (5), No. 1703878.
(18) Chaudhary, K. Polariton nanophotonics using phase-change materials. *Nat. Commun.* **2019**, DOI: 10.1038/s41467-019-12439-4.
(19) Bauters, J. F.; et al. Planar waveguides with less than 0.1 dB/m propagation loss fabricated with wafer bonding. *Opt. Express* **2011**, *19* (24), 24090−24101.
(20) Zheng, J.; et al. GST-on-silicon hybrid nanophotonic integrated circuits: a non-volatile quasi-continuously reprogrammable platform. *Opt. Mater. Express* **2018**, *8* (6), 1551−1561.
(21) Delaney, M.; Zeimpekis, I.; Lawson, D.; Hewak, D. W.; Muskens, O. L. A New Family of Ultralow Loss Reversible Phase-Change Materials for Photonic Integrated Circuits: Sb2S3 and Sb2Se3,″ (in English). *Adv. Funct Mater.* **2020**, DOI: 10.1002/adfm.202002447.
(22) Ríos, C.; et al. Ultra-compact nonvolatile phase shifter based on electrically reprogrammable transparent phase change materials. *PhotoniX* **2022**, *3* (1), 26.
(23) Fang, Z.; et al. Ultra-low-energy programmable non-volatile silicon photonics based on phase-change materials with graphene heaters. *Nat. Nanotechnol.* **2022**, *17* (8), 842−848.
(24) Delaney, M.; et al. Nonvolatile programmable silicon photonics using an ultralow-loss Sb2Se3 phase change material. *Science Advances* **2021**, *7* (25), No. eabg3500.
(25) Fang, Z.; Zheng, J.; Saxena, A.; Whitehead, J.; Chen, Y.; Majumdar, A. Non-Volatile Reconfigurable Integrated Photonics Enabled by Broadband Low-Loss Phase Change Material. *Advanced Optical Materials* **2021**, DOI: 10.1002/adom.202002049.
(26) Qiu, F. Ultra-thin silicon/electro-optic polymer hybrid waveguide modulators. *Appl. Phys. Lett.* **2015**, DOI: 10.1063/1.4931490.
(27) Rahim, A.; Spuesens, T.; Baets, R.; Bogaerts, W. Open-Access Silicon Photonics: Current Status and Emerging Initiatives. *Proceedings of the IEEE* **2018**, *106* (12), 2313−2330.
(28) Liddle, J. A.; Bowser, J.; Ilic, B. R.; Luciani, V. ″So, You Want to Have a Nanofab? Shared-Use Nanofabrication and Characterization Facilities: Cost-of-Ownership, Toolset, Utilization, and Lessons Learned,″ (in eng). *J. Res. Natl. Inst Stand Technol.* **2020**, *125*, No. 125009.

https://doi.org/10.1021/acs.nanolett.4c00070
Nano Lett. 2024, 24, 6844−6849